Midwave-Infrared Snapshot Imaging Spectrometer

Curtis E. Volin, John P. Garcia, Eustace L. Dereniak, Michael R. Descour

Optical Sciences Center, University of Arizona, Tucson, AZ 85721

Tom Hamilton, Robert McMillan

SMDC-TSC, 106 Wynn Dr., Huntsville, AL 35805

ABSTRACT

We report results from a demonstration of a midwave-infrared non-scanning, high speed imaging spectrometer capable of simultaneously recording spatial and spectral data from a rapidly varying target scene. High speed spectral imaging was demonstrated by collecting spectral and spatial snapshots of blackbody targets and combustion products. The instrument is based on computed tomography concepts and operates in a mid-wave infrared band of 3.0 to 5.0 μm. Raw images were recorded at a frame rate of 60 fps using a 512 × 512 InSb focal plane array. Reconstructed object cube estimates were sampled at 46×46×21 (x, y, λ) elements, or 0.1 μm spectral sampling. Reconstructions of several objects are presented.

1. INTRODUCTION

An imaging spectrometer measures both the spatial and spectral content of an object scene. In contrast with classical, broadband imaging, the spectral information permits the classification of portions of the scene based upon material content or temperature. The 3D (x, y, λ) object for an imaging spectrometer is referred to here as the *object cube*.

This project concerns imaging spectrometry in the mid-wave infrared (MWIR) spectral region. Mid-wave refers to the atmospheric window which exists at wavelengths between 3.0 μm and 5.0 μm. Outside this passband absorption renders even a short path through the atmosphere completely opaque.

The computed-tomography imaging spectrometer (CTIS) employs a very simple optical system in order to measure the object cube *without any scanning*. The object cube is not measured directly, but in a manner that requires complicated post-processing to extract an estimate of the object's 2D spectral radiance. Therefore, in contrast to the classical scanning imaging spectrometers, the CTIS is a *snapshot instrument*. [1,2]

The target application of the CTIS is a spatially non-localized or spatially complex, dynamic event which contains thermal or chemical structure which may be explored via the spectral radiance of the event. The application of a standard scanning spectrometer to such targets could either miss the event or return data corrupted by temporal artifacts.

For example, the visible-wavelength CTIS has been applied in the field to imaging of missiles in flight. Following this course, the impact of missiles or other projectiles presents another application for CTIS over purely imaging system or conventional imaging spectrometers. Recording of a full object cube sequence allows observation of the physical, thermal, and chemical evolution in time of the event in two dimensions. The CTIS' potential to recover chemical and thermal information via spectral content also extends to explosions, plumes, exhausts, or flares.

Imaging Spectrometry VII, Michael R. Descour, Sylvia S. Shen, Editors,
Proceedings of SPIE Vol. 4480 (2002) © 2002 SPIE · 0277-786X/02/$15.00

2. MWIR CTIS INSTRUMENT

The driving concept behind the development of the CTIS is the reconstruction of a 3D object from multiple 2D projections. If sufficient projections are recorded, then the original object cube can be reconstructed. These projections are shown schematically in Figure 1. A two dimensional array records these many projections, and reconstruction of the (x, y, λ) object is accomplished via inversion methods.[2]

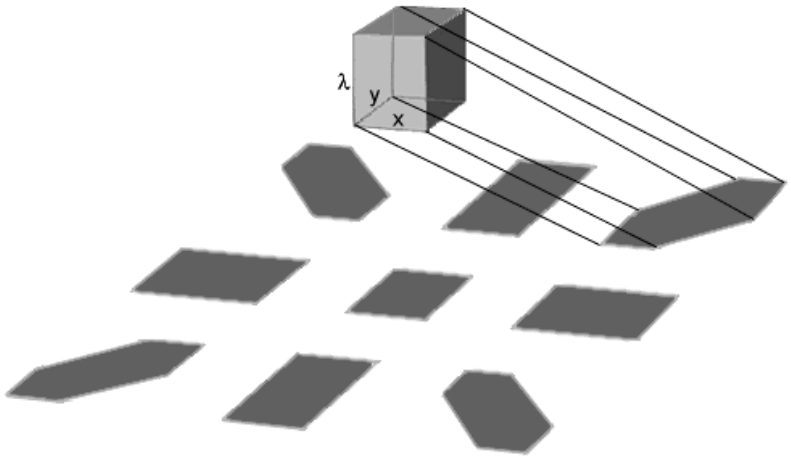

Figure 1. Projections of the object cube. Spectral information along the vertical axis of the object cube is projected along the radial coordinate of the focal plane and multiplexed with spatial information.

The computed tomography imaging spectrometer consists of three optical-element groups: an objective lens, a collimation lens, and a re-imaging lens (Figure 2). The Computer Generated Hologram (CGH) disperser is located in collimated space between the collimator lens and the re-imaging lens. The large-format focal plane array (FPA) is conjugate to the field stop.

The MWIR CTIS, shown in Figure 2, uses a 512 x 512 pixel InSb array with 25 μm pitch operating at 60 frames per second with variable integration time. The 5 mm square field stop maps to an 46×46 pixel area on the focal plane array. The system uses a 100 mm reimaging lens and a 500 mm collimating lens.

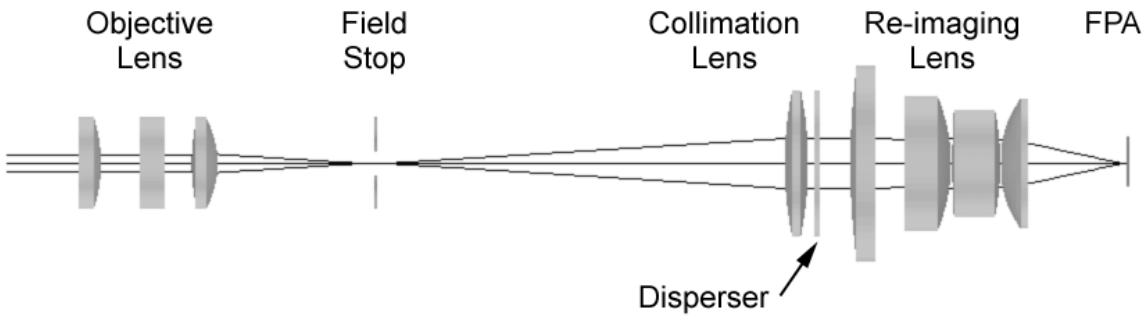

Figure 2. Optical schematic of the CTIS including the chief ray.

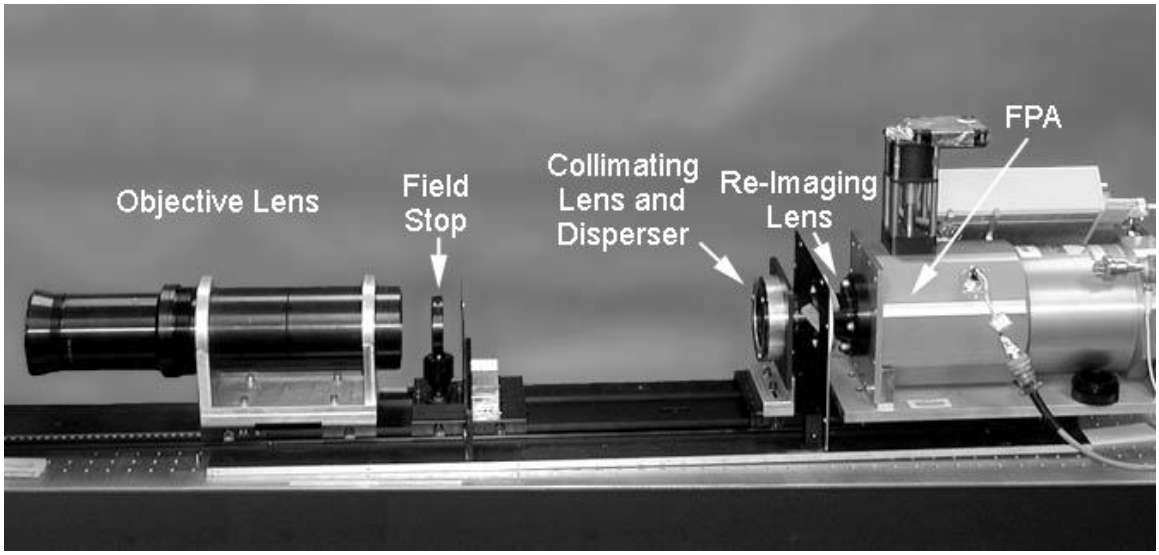

Figure 3. MWIR CTIS instrument.

Without a CGH, the optical system images the field stop at small magnification onto the focal plane array, so that only a small portion of the FPA is dedicated to sampling the field-of-view. The introduction of the CGH causes light to be dispersed into many additional images on the FPA. The particular design of the CTIS CGH forms a square array of equi-spaced *diffraction orders*. An example MWIR CTIS image of a monochromatic, point object is shown in Figure 4(a).

Each diffraction order is subject to dispersion (with the exception of the center order), which causes the order to exhibit a linear blur. The dispersion blur for a particular order is oriented along the same direction as the diffraction. This blur can be observed in Figure 4(b), an image of a uniform, warm source. Each blurred image may be expressed as the 2D recording of a projection through the object cube.

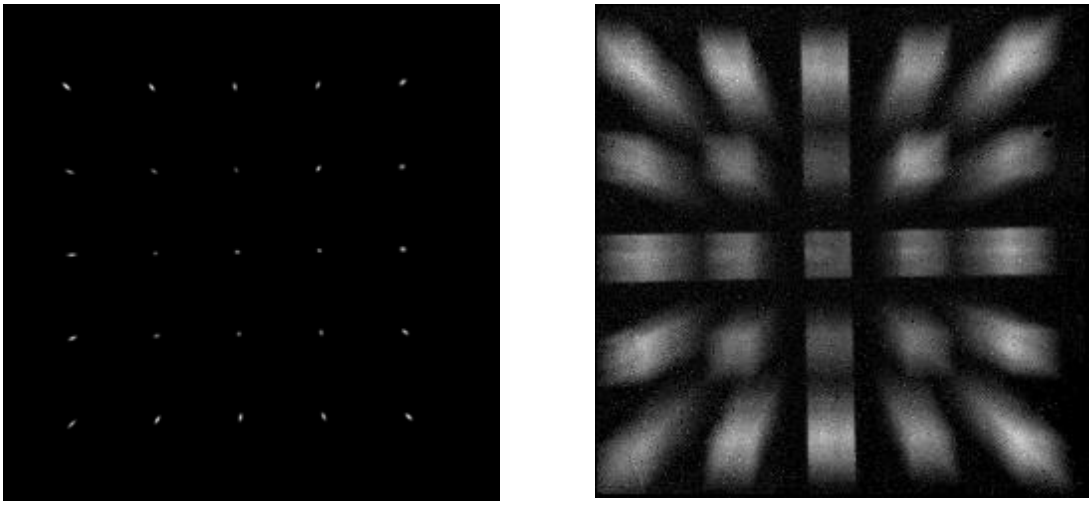

(a) (b)

Figure 4. MWIR CTIS images; (a) Raw image of a narrowband, point source, (b) Raw image of a uniform, broadband source.

3. CGH DISPERSER

The CGH disperser used in the CTIS is composed of a square unit cell identically repeated over a large area. Each cell contains an integral number of square pixels, each of which has a uniform depth (see Figure 5). This type of CGH, when inserted into the CTIS optical system, causes light from a monochromatic point-source in the field stop to separate into an equi-spaced, square grid of discrete points, or diffraction orders, on the FPA [see Figure 4(a)].[3]

The CGH disperser used in the MWIR CTIS is designed to produce uniform peak irradiance into each of the 5×5 projections on the focal plane for a spatially and spectrally extended object. Since increasing dispersion causes projections to spread over a larger area of the FPA, the higher diffraction orders are assigned greater efficiency to maintain uniform irradiance. Furthermore, the diffraction efficiency as a function of wavelength is designed to be uniform in each order. A detailed description of the CGH design process and an examination of the fabricated CGH are presented in another paper within this conference.[4]

The CGH cell is 190 μm square and contains 10×10 pixels. The depths have been discretized to 16 equally spaced levels for fabrication in GaAs using multiple-mask lithography and reactive-ion beam etching. The maximum etch depth was 2.73 μm. The fabrication was performed at Sandia National Laboratories. A WYKO NT2000[5] depth measurement of a small portion of the fabricated CGH is shown in Figure 5.

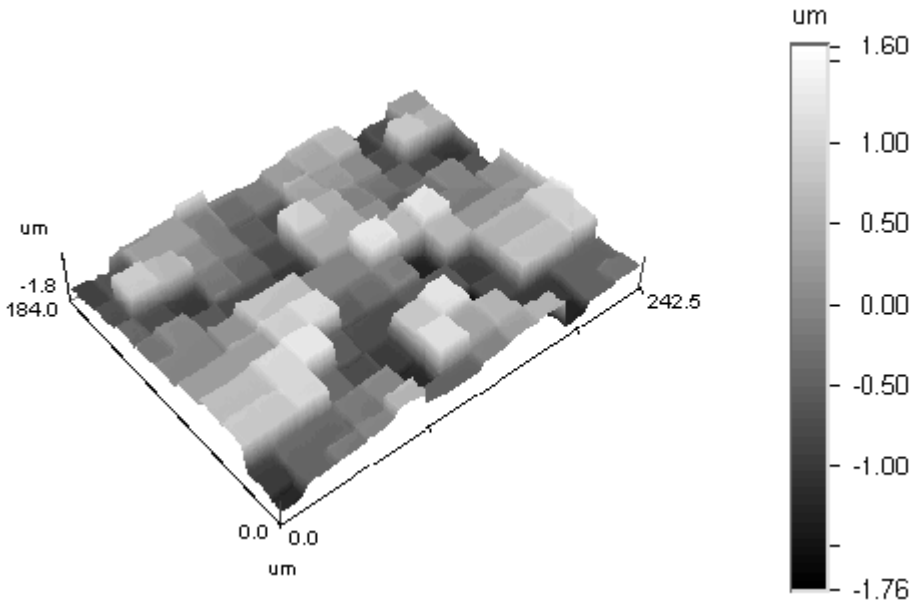

Figure 5. Topography measurement of a segment of the fabricated uniform-irradiance CGH.

4. CALIBRATION

The CTIS "calibration" is not just a calibration in the traditional sense associated with spectrometers, i.e. converting ADUs from the CCD into radiometric units or assigning spectral units to the detector bins. The CTIS multiplexes spatial and spectral data in a manner which defies direct interpretation of the resulting raw image in terms of spectra and spectral images.

The object cube estimate is discretized into a contiguous set of (Δx, Δy, $\Delta\lambda$) volume elements, of *voxels*. The calibration of the CTIS must quantify how each voxel is mapped onto the FPA, including not just the location of the diffraction orders but also effects from wavefront aberrations, distortion, diffraction, spectral transmission, internal reflections, and pixel fill factor. The end result of calibration is the system

matrix, which will be employed by the reconstruction algorithms (described below) to recover an object cube estimate from a raw image.

Calibration is performed experimentally for the MWIR CTIS. Experimental calibration requires direct measurement of the voxel spread function (VSF) of each voxel in the object cube estimate. This measurement task is prohibitively large (for both time and storage) since recent MWIR instruments have up to $46 \times 46 \times 21$ sampling, or about 44,000 voxels. However, the field stop occupies only a small area on the focal plane array. If the optical system is sufficiently isoplanatic over regions of the size of the field stop, only one VSF for each wavelength actually needs to be experimentally measured and the rest are generated by shifting the measured VSFs.[6]

A voxel is simulated by a source of the same approximate spatial size and spectral bandwidth. The calibration setup used to create such a source is shown in Figure 6. All shields and baffles around the CTIS and reference detector were removed for the picture. The aperture of a 1000 K blackbody is imaged onto the entrance port of a 4.0-μm blazed-grating monochromator. The monochromator exit port of is imaged onto a 100 μm diameter As-Se-Te fiber-optic waveguide. The fiber features a wide absorption band in the 4.2-4.8 micron range, therefore, a short (1/2 m) length of fiber was used to decrease the integrated absorption.[7] A Ge singlet lens (25 mm effective-focal-length) is used to image the fiber optic output into the field stop of the CTIS.

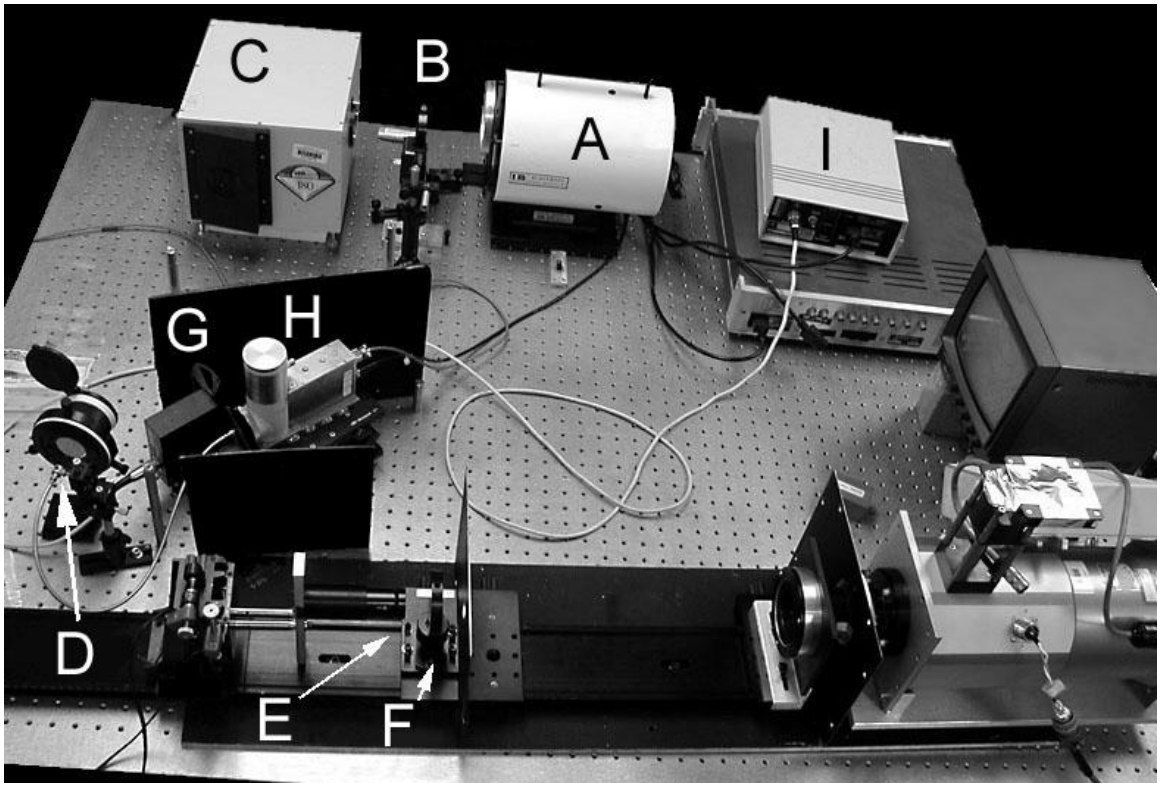

Figure 6. MWIR CTIS calibration setup pictured with the CTIS. A: blackbody source; B: lens; C: monochromator; D: Fiber optic waveguide input face; E: Fiber imaging lens; F: CTIS field stop; G: chopper wheel; H: HgCdTe reference detector; I: Chopper controller and lock-in amplifier. The fiber-waveguide output is positioned for the reference detector measurement.

A HgCdTe photovoltaic detector cooled to 77K is used as a radiance reference detector for normalization of the calibration images. The detector operates in a nearly flat regime of photon response over the 3.0-5.0 μm range.[8] A chopper wheel inserted at the end of the fiber optic waveguide isolates the voxel light from background. The signal is read out through a lock-in amplifier. An example reference

measurement is shown in Figure 7. The CO_2 absorption band (4.2-4.3 μm) and the fiber-waveguide absorption band (4.5-4.8 μm) are indicated by the gray bands in the plot. The calibration images are normalized by the reference detector measurement so that the reconstructed object cube estimates have units *proportional to* photons.

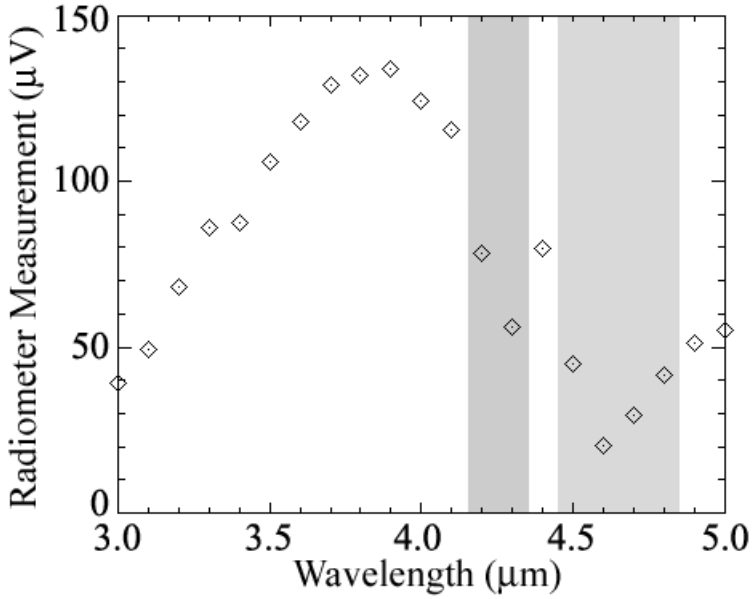

Figure 7. Reference detector measurement for the MWIR CTIS calibration. Gray bars indicate the CO_2 absorption band (4.2-4.3 μm) and the fiber-waveguide absorption band (4.5-4.8 μm).

Measured VSFs for several wavelengths are shown in Figure 8. Note the large amount of pincushion distortion in the 5.0 μm VSF. With regard to the impact of distortion on the shift-invariance of the CTIS, the most important figure-of-merit is the maximum error in location due to the local distortion within a single field stop projection at a single wavelength. The maximum error occurs at the highest-field-angle location in the image, the upper-right corner of the (2, 2) diffraction order at 5.0 μm. The amount of distortion can be easily calculated from the calibration images. The calculated error is about 1.7 pixels between the actual diffraction spot location and the expected location (from shifting the 5.0 μm VSF from the center of the field stop).

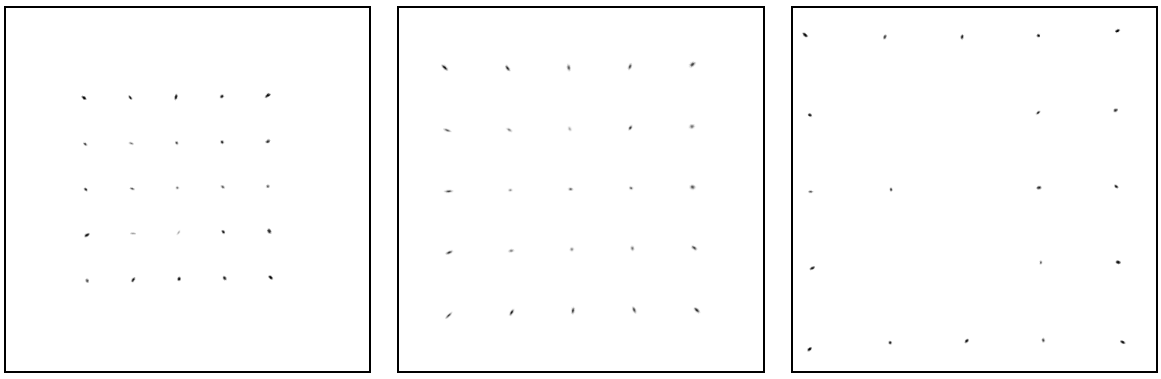

3.0 μm 4.0 μm 5.0 μm

Figure 8. MWIR CTIS calibration images at three selected wavelengths (contrast inverted).

Reduction of error caused by distortion may be handled in the reconstruction process. Due to the 3rd-order field-angle dependence of the distortion, the maximum error is reduced to just one pixel by thresholding the raw image at a field angle corresponding to the width of the FPA. That is, a round aperture with diameter equal to the FPA size is imposed upon the recorded image and all pixels outside the aperture are not used in reconstruction.

5. RECONSTRUCTION

Reconstruction employs the Expectation Maximization (EM) iterative algorithm to calculate an object cube estimate from a raw image.[9] All reconstructed object cube estimates presented here have 46×46×21 sampling, or 0.1 μm spectral intervals through the 3.0 - 5.0 μm wavelength range. Each iteration of the reconstruction algorithms takes approximately five seconds for 46×46×21 (x, y, λ) sampling.[10] Typically, four to ten EM iterations are required to complete a reconstruction. The specific number of iterations is adjusted manually depending upon the spatial and spectral complexity of the object.

6. RESULTS

Three representative targets have been examined to provide a broad study of the instrument's reconstruction capabilities. The first target examined consists of a warm (~150º C), flat-black panel obscured by a filter wheel. The raw image is shown in Figure 9. The upper filter cell contains a broadband (3.4 - 3.9 μm FWHM) pass filter and the rightmost filter cell provides a direct view of the warm panel. A HeNe laser spot (3.39 μm) illuminates the hub of the filter wheel.

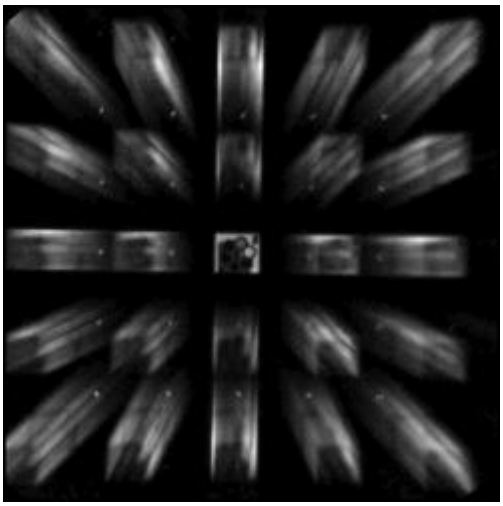

Figure 9. Raw image of the broadband filter target.

The reconstruction shown in Figure 10 was calculated using ten iterations of EM. The spectral images are organized by increasing wavelength from the lower left. The laser spot is clearly visible in the 3.4 μm image and the broadband filter reconstructs in the appropriate spectral images.

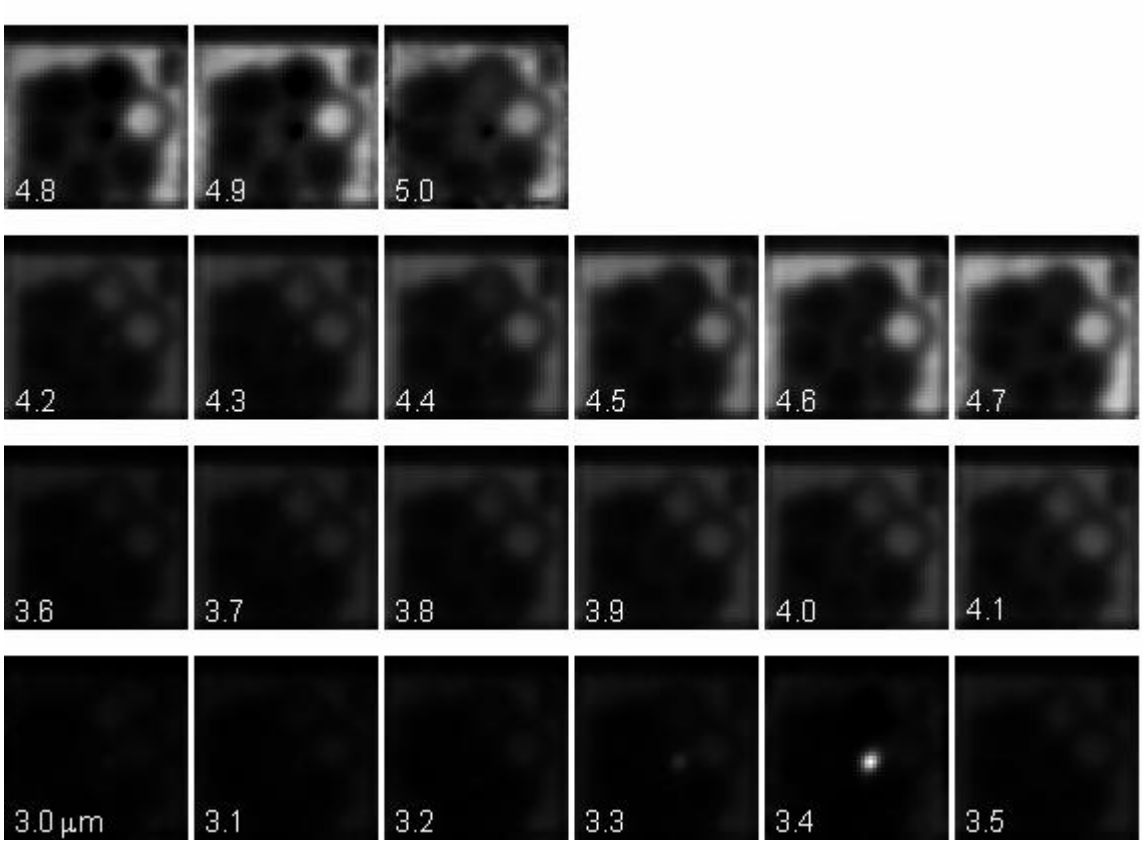

Figure 10. Spectral images from a reconstruction of the broadband filter target.

The second target is intended to demonstrate the accuracy of the spectral calibration of the MWIR CTIS. The object is a small-aperture 400°C blackbody. The raw image (with the center order truncated) can be seen in Figure 11(a). The reconstruction used six iterations of EM. The 4.0 μm spectral image is shown in Figure 11(b) and the reconstructed spectral radiance from the brightest spatial resolution element is shown in Figure 11(c). The gray line in the spectral radiance plot is proportional to the 400ºC blackbody photon emission profile. The constant of proportionality was chosen to minimize the sum of the squared error between the emission profile and the reconstructed spectrum. Significant discrepancies between the reconstruction and blackbody radiance occur in the 4.2-4.3 μm absorption band, the 4.5-4.6 band, and at the extreme edges of the reconstruction, as indicted by the bands in the plot. These discrepancies are attributed to CO_2 absorption in the optical path for the 4.2-4.3 μm band, low SNR in the calibration images near the fiber absorption line (4.5 μm) and at short wavelengths (3.0-3.1 μm) and the cut-off of the camera's band-pass filter in the middle of the 5.0 μm band.

(a) (b)

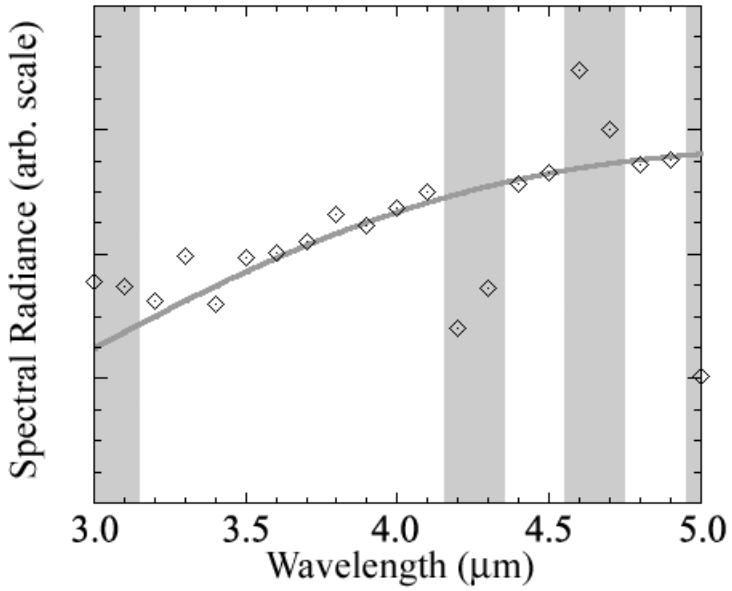

(c)

Figure 11. 400°C blackbody reconstruction results; (a) raw image, (b) reconstructed spectral image at 4.0 μm, (c) spectrum plotted from the brightest spatial position in the spectral image. The line is proportional to the 400°C blackbody photon emission profile. Gray bars indicate regions of great discrepancy, as described in the text.

The third representative target demonstrates the temporal resolution of the CTIS. The target consists of a burning match viewed through an attenuating filter. A diagram of the target is shown in Figure 12. After burning for several seconds, the spectral emission of the scene contains two different spectral species, the first from the smoldering match (peak at 4.9 μm) and the second due to emission from hot CO_2 gas (peak at 4.4 μm).

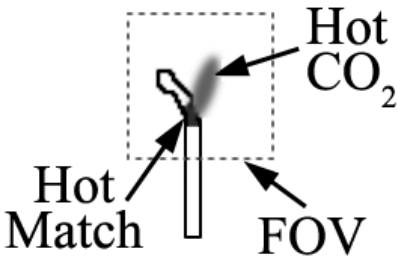

Figure 12. Diagram depicting the arrangement of the match and flame in the burning-match target.

Seven iterations of EM were used for the reconstruction. The spectral images are shown in Figure 13. The flame is brightest in the 4.4 μm spectral image while the smoldering match appears brighter in the 4.9 μm spectral image. Figure 14 shows the spectra from a point near the center of the flame [Figure 14(a)] and a point near the center of the match [Figure 14(b)].

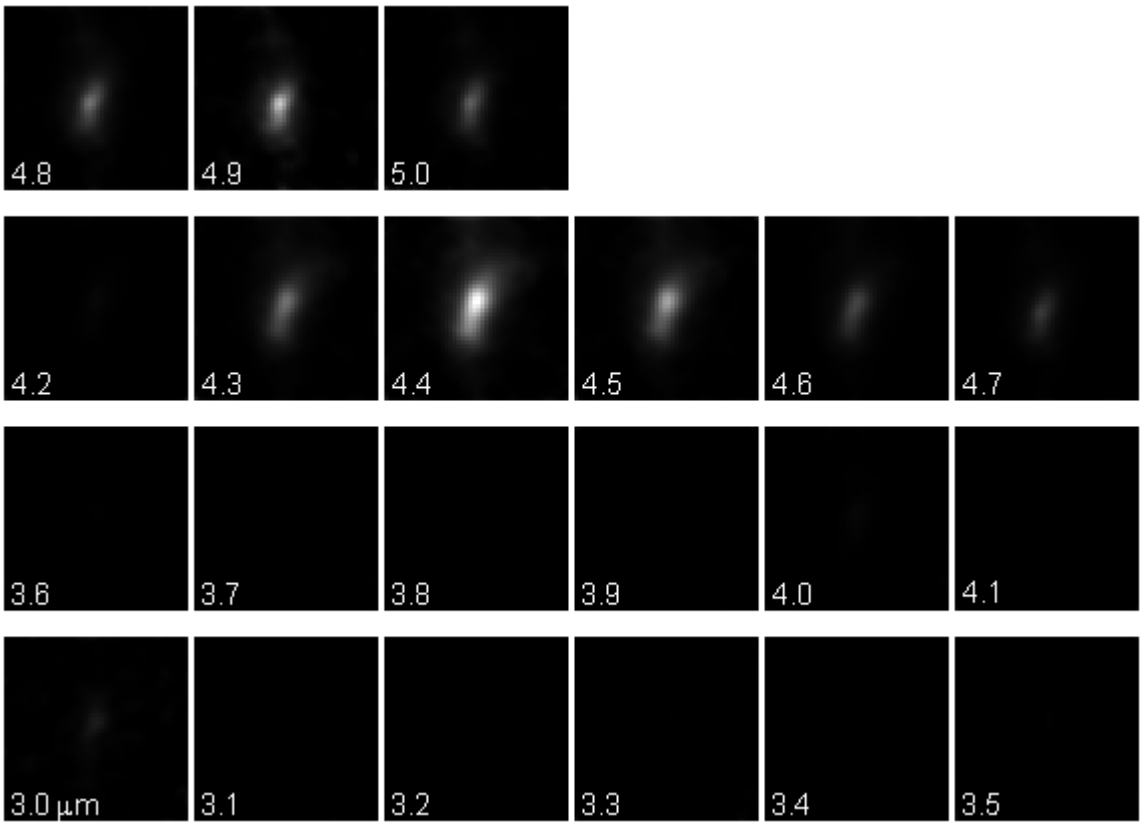

Figure 13. Spectral images from the reconstruction of the burning match target. The diagram in Figure 13 indicates the arrangement of the match and flame.

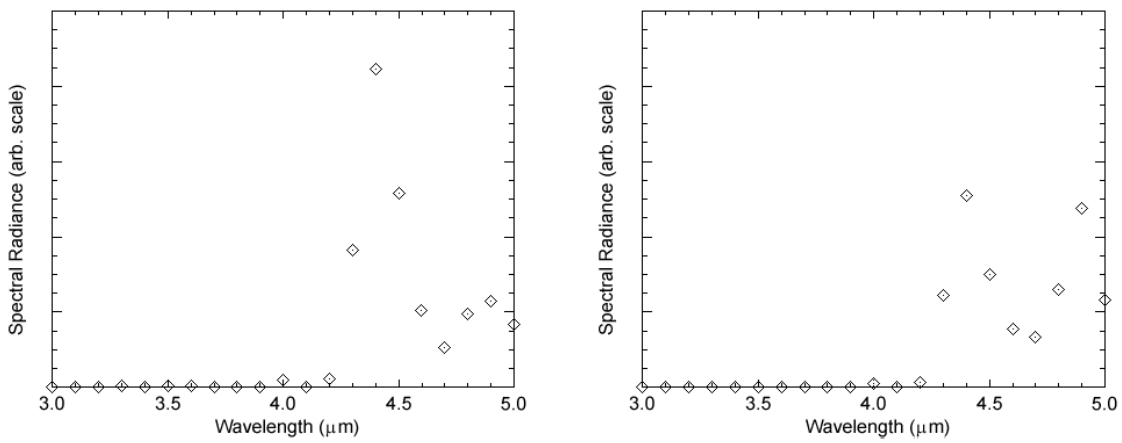

(a) (b)

Figure 14. Spectra from selected positions in the burning match reconstruction.

7. CONCLUSIONS

A practical, field-capable, 3.0 to 5.0 μm mid-wave infrared computed-tomography imaging spectrometer has been demonstrated. Results were presented for reconstructions of laboratory targets with sampling up to 46×46×21 voxels in the reconstructed object cube, or 0.1 μm spectral sampling. Demonstration of the snapshot capability has been performed on both static targets and targets with rapidly varying content. This instrument offers snapshot spectral imaging capabilities which are not reproducible by other spectrometers due to their need for scanning.

The calibration procedures have been revised so that the reconstructed spectra are normalized to units proportional to photons. Further improvement in reconstruction accuracy requires the use of a brighter blackbody source to increase SNR in the experimental calibration.

Several improvements to the CTIS instrument and calibration system are still needed. The CTIS hardware should be improved by replacing the collimating singlet with a doublet and cooling the field stop. In the calibration system, the Ge singlet fiber-imaging lens should be replaced with an achromatic doublet. Hardware control and automation procedures must be developed to increase the speed of calibration.

ACKNOWLEDGEMENTS

The authors would like to thank Shanalyn Kemme, G. Allen Vawter, Charles R. Alford, and Sandy Samora at Sandia National Labs for laying out and fabricating the CGH disperser.

REFERENCES

1. M. R. Descour, "Non-scanning imaging spectrometry," Ph.D. Dissertation, University of Arizona (1994).

2. M. R. Descour and E. L. Dereniak, "Computed-tomography imaging spectrometer: experimental calibration and reconstruction results," *Applied Optics* **34**, 4817-4826 (1995).

3. Christopher Coleman, "Computer Generated Holograms for free-space optical interconnects," Ph.D. Dissertation, University of Arizona, Chapter 3 (1998).

4. Curtis E. Volin, Michael R. Descour, Eustace L. Dereniak, “Design of broadband-optimized computer-generated hologram dispersers for the computed-tomography imaging spectrometer,” in *Imaging Spectrometry VII*, Michael R. Descour, Sylvia S. Shen, eds., Proc. SPIE 4480 (2001).

5. Veeco Instruments, Corp, Tucson, AZ.

6. C. E. Volin, B. K. Ford, M. R. Descour, J. P. Garcia, D. W. Wilson, P. D. Maker, “High speed spectral imager for imaging transient fluorescence phenomena”, Applied Optics **37**, No. 34 (Dec. 10, 1998).

7. Amorphous Materials Inc., 3130 Benton, Garland, TX 75042.

8. SBRC Infrared Wall Chart (1984).

9. L. A. Shepp and Y. Vardi, “Maximum Likelihood reconstruction for emission tomography,” *IEEE Trans. Med. Imaging*, MI-1, No. 2, pp. 113-122 (1982).

10. Curtis E. Volin, "Portable Snapshot Infrared Imaging Spectrometer," Ph.D. Dissertation, Chapter 4, pp. 66-81, University of Arizona (2000).